The American Journal of Human Genetics, Volume *100*

Supplemental Data

Mutations in *MAPKBP1* Cause Juvenile or Late-Onset Cilia-Independent Nephronophthisis

Maxence S. Macia, Jan Halbritter, Marion Delous, Cecilie Bredrup, Arthur Gutter, Emilie Filhol, Anne E.C. Mellgren, Sabine Leh, Albane Bizet, Daniela A. Braun, Heon Y. Gee, Flora Silbermann, Charline Henry, Pauline Krug, Christine Bole-Feysot, Patrick Nitschké, Dominique Joly, Philippe Nicoud, André Paget, Heidi Haugland, Damien Brackmann, Nayir Ahmet, Richard Sandford, Nurcan Cengiz, Per M. Knappskog, Helge Boman, Bolan Linghu, Fan Yang, Edward J. Oakeley, Pierre Saint Mézard, Andreas W. Sailer, Stefan Johansson, Eyvind Rødahl, Sophie Saunier, Friedhelm Hildebrandt, and Alexandre Benmerah

Supplemental figures

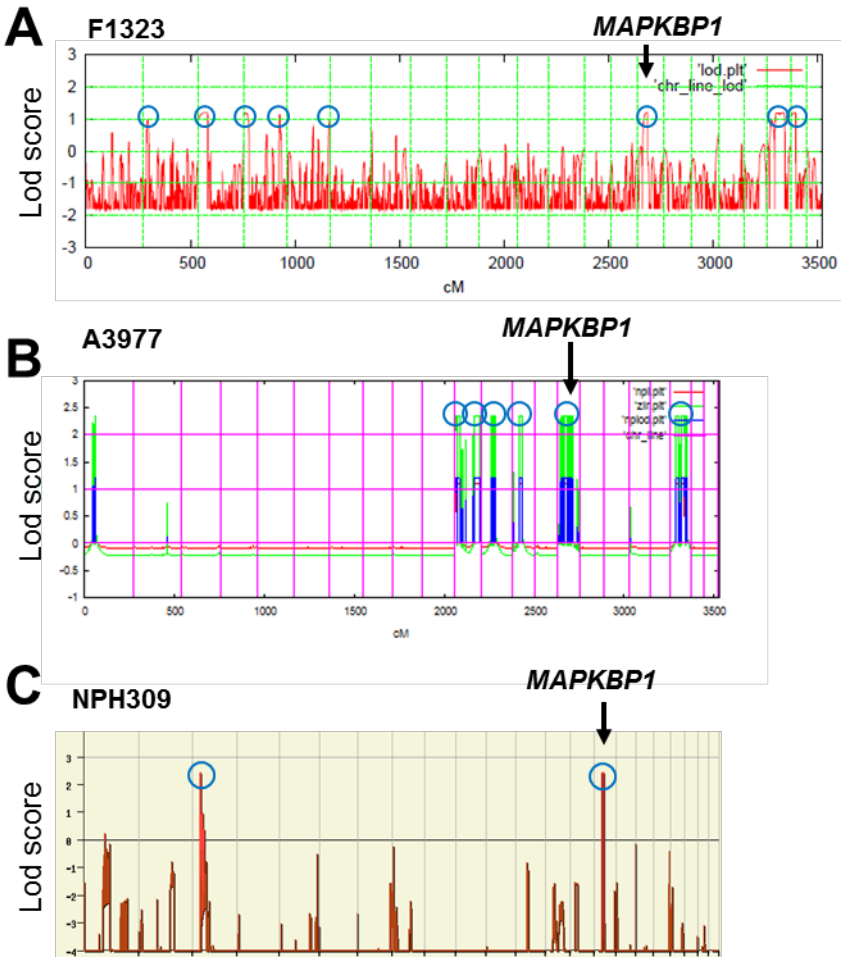

Figure S1: Homozygosity mapping in families F1323, A3977 and NPH309.
For genome-wide homozygosity mapping GeneChip® Human Mapping 250k StyI Array (Affymetrix) was used. Non-parametric LOD scores were identified using MERLIN software for NPH309 and GENEHUNTER 2.1 (PMID: 8651312 / PMID: 10796874) through stepwise use of a sliding window with sets of 110 SNPs and the program ALLEGRO (PMID: 10802644) in order to identify regions of homozygosity, using a disease allele frequency of 0.0001 and Caucasian marker allele frequencies. For graphical presentation nonparametric lod scores (NPL) were calculated and plotted across the human genome. The x axis shows Affymetrix 250K StyI array SNP positions on human chromosomes concatenated from p-ter (left) to q-ter (right). Genetic distance is given in cM. Note that the locus of MAPKBP1 resides within one of the homozygous regions on chromosome 15 (black arrow).

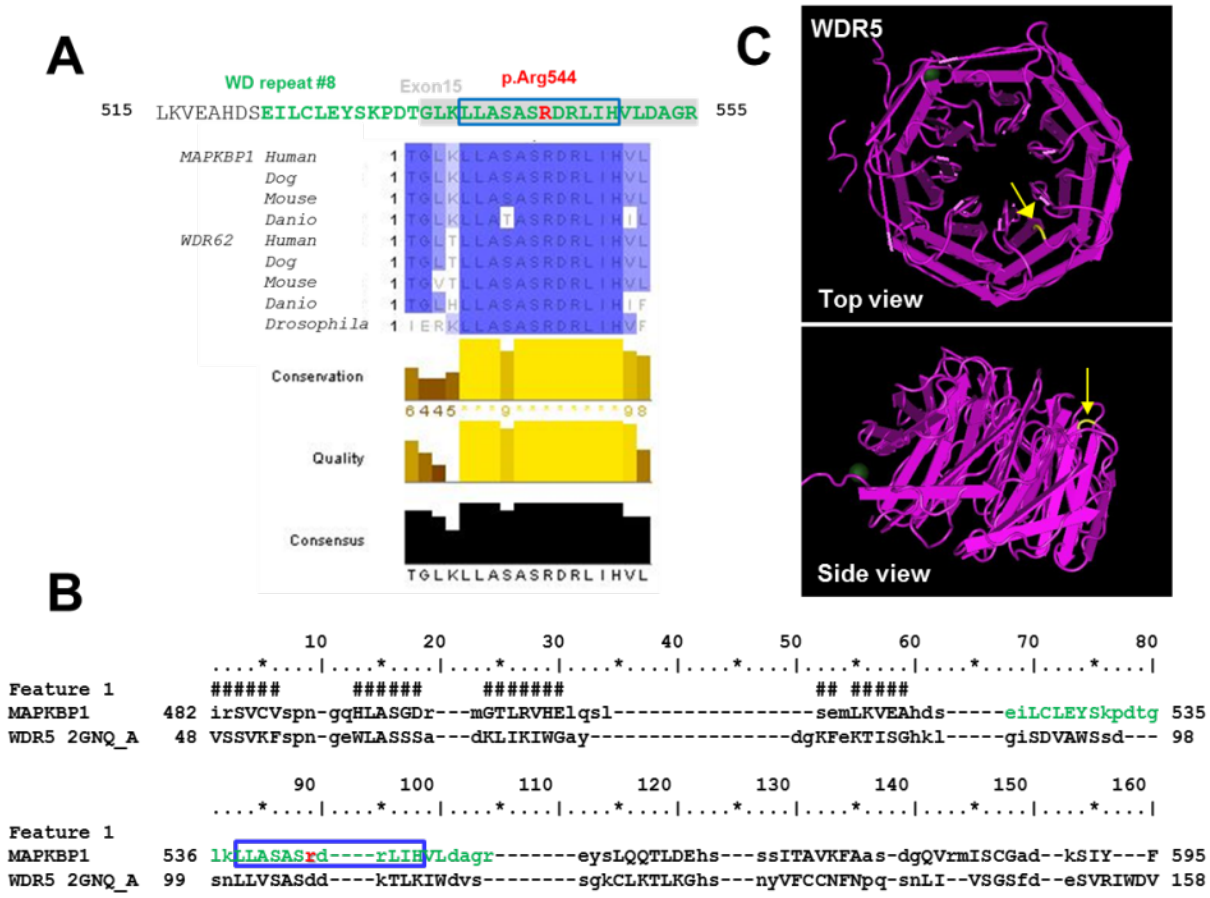

Figure S2: Arg544 is a highly conserved residue likely involved in protein-protein interaction of the WD domain.

A) The Arg544 residue (red) mutated in the NPH2139 family is found in a 12 amino-acid region (boxed in blue) within the eighth WD repeat (green) which is highly conserved among species in both MAPKBP1 and WDR62 as well as in the unique ortholog in *Drosophila*. Sequence alignment was made using Jalview (http://www.jalview.org/). **B)** BLAST and CDD analysis at NCBI revealed that the 8th WD repeat containing the Arg544 residue shows some similarity with one of the WD repeat from the WDR5 protein, which structure has been solved[1]. **C)** Analysis of the 3D structure of the whole WD domain of WDR5 using Cn3D 4.3 (http://www.ncbi.nlm.nih.gov/Structure/CN3D/cn3d.shtml; 2GNQ_A) indicates that the D107 (yellow) corresponding to Arg544 in MAPKBP1 (red) is pointing toward the "top" of the blade and was shown to be required for the interaction of WDR5 with Histone H3[2].

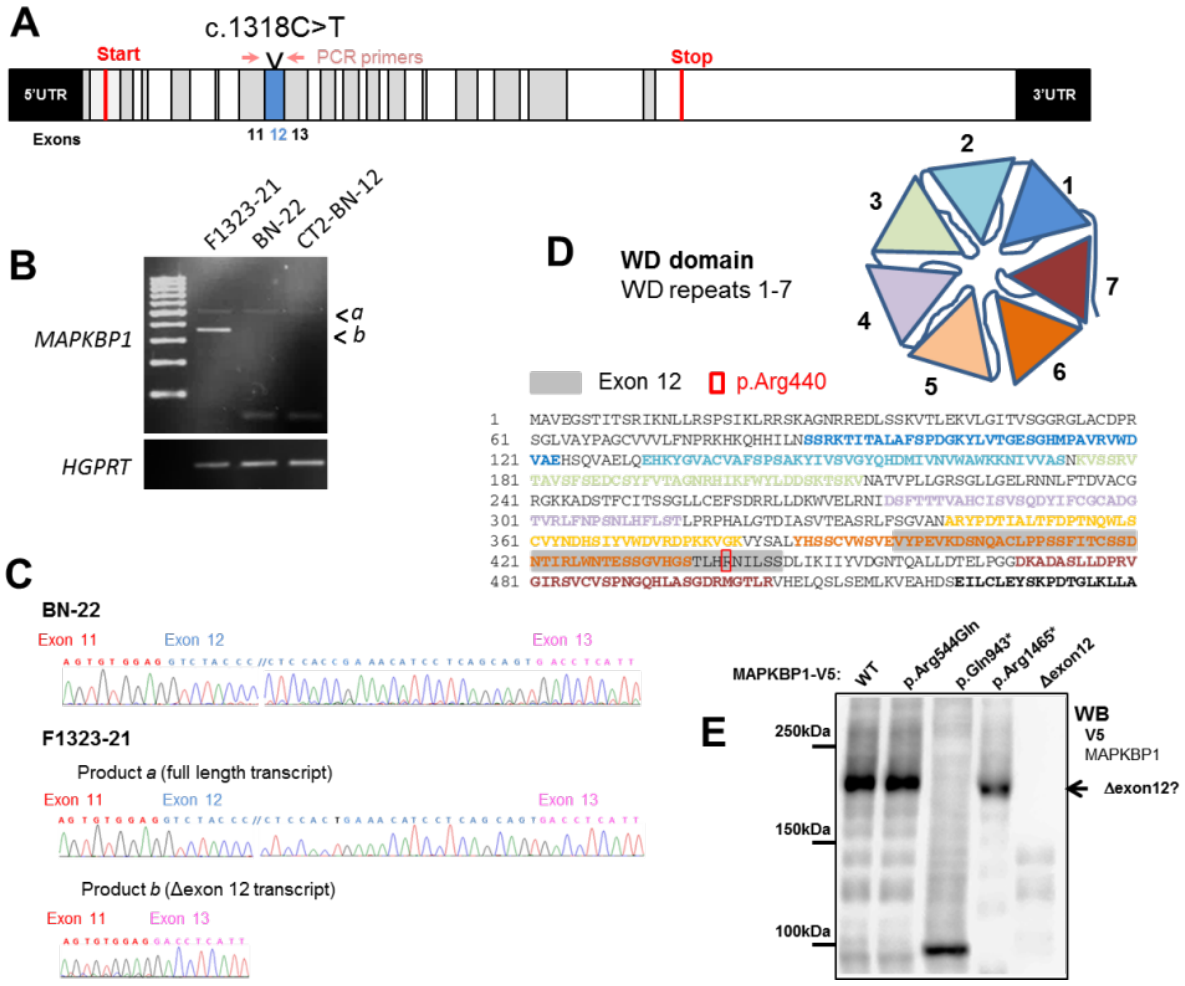

Figure S3: Exon 12 is skipped in F1323-21 individual homozygous for the c.1318C>T mutation.

A) Primers in exons 11 and 13 were designed to amplify exon 12 in which the c.1318C>T mutation is present (MKBP1-primer-11F: 5'-TCTTCTCTGGAGTGGCGAATG-3', MKBP1-primer-13R: 5'-TAAGTGTGCCCATACGGTCCG-3'). **B**) The 11-13 exon region was amplified by RT-PCR from RNA isolated from cycling fibroblasts from F1323-21 and BN-22 affected individuals as well as from control individual CT2-BN-12 (mother of BN-22; see Fig.1). Two PCR products were amplified from the F1323-21 individual samples, one of the expected size also found in the other individuals (product a) and one smaller fragment only found in this affected individual (product b). **C**) RT-PCR products from BN-22 and F1323-21 individuals were sequenced by Sanger and corresponding chromatograms are shown with the mutated nucleotide indicated in black. **D**) Scheme showing the organization of a typical WD domain which is composed of 7 WD repeats and sequence of the N-terminal WD domain of MAPKBP1 where each of the first 7 WD repeats is in the same color as in the scheme. The p.Arg544 residue is boxed in red and exon 12 encoded region in grey. **E**) Lysates of HEK293 cells transiently transfected with the indicated V5-tagged MAPKBP1 encoding plasmids were analyzed by western-blot (WB) using the rabbit polyclonal antibody against the V5 epitope (see **Figure S6**). Expected size of the Δexon12 is indicated by an arrow.

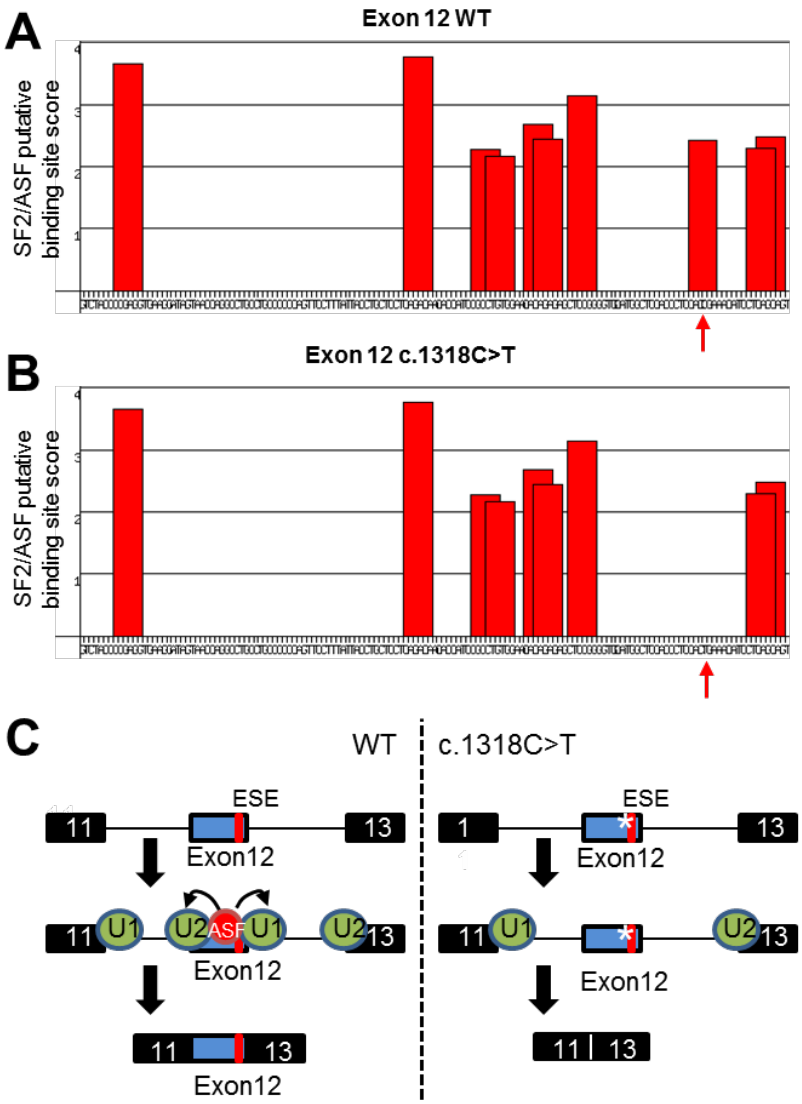

Figure S4: The c.1318C>T mutation in exon 12 is predicted to affect a SR protein binding site.

A-C) Sequence of WT (**A**) and mutated (**B**) exon 12 were subjected to ESEfinder (http://krainer01.cshl.edu/cgi-bin/tools/ESE3/esefinder.cgi?process=home)[3] to check for putative binding of serine-arginine rich (SR) proteins on exonic splicing enhancer (ESE) which then bind to splicing factors (U; **C**). ESEfinder analysis revealed that the c.1318C>T mutation affects one putative binding site for SF2/ASF and is therefore likely to increase the probability of skipping of exon 12 (red arrow).

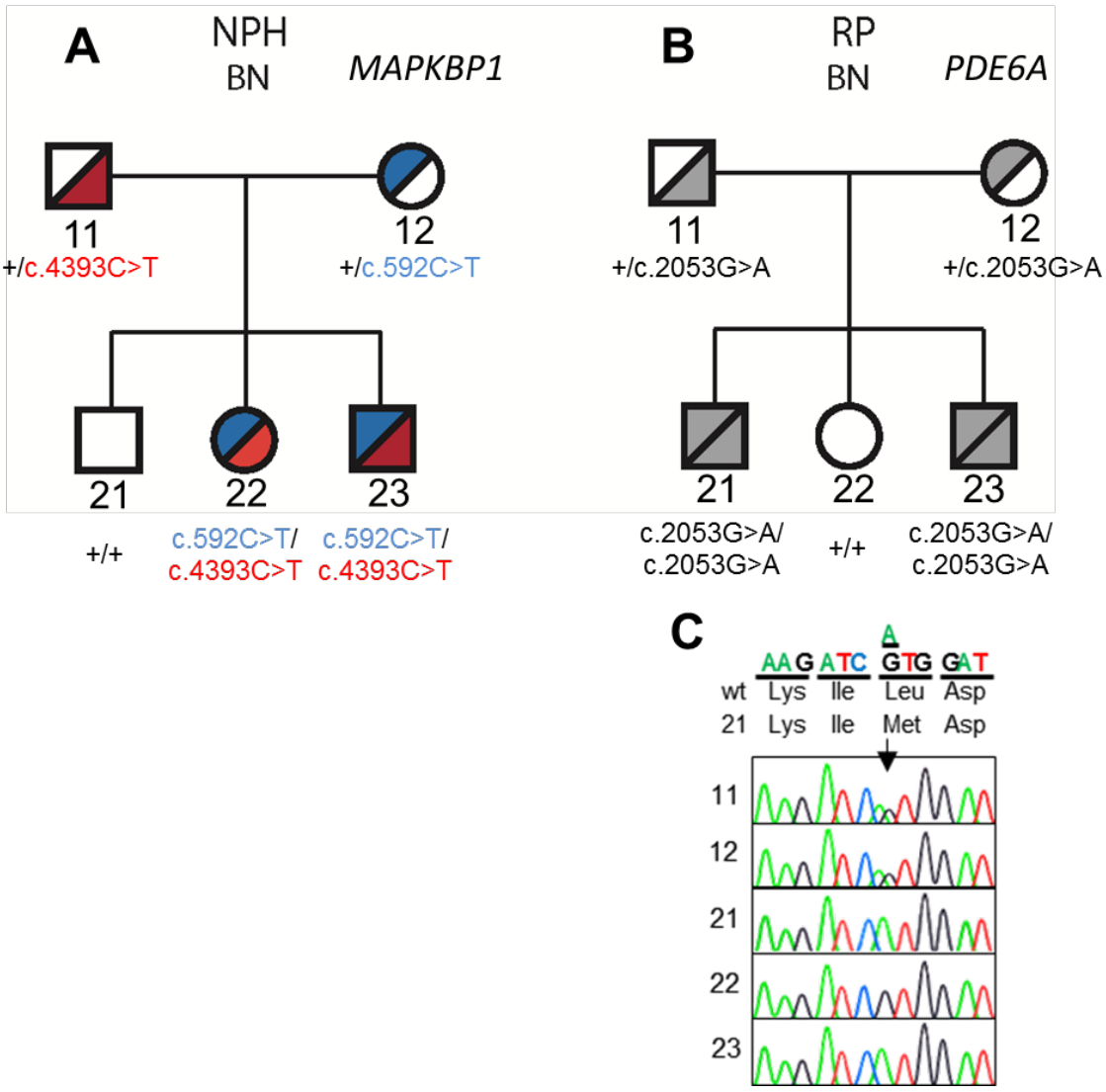

Figure S5: Segregation of nephronophthisis and retinitis pigmentosa in the BN family.

A-B) The affected individuals BN-22 and BN-23 were compound heterozygous for mutations in *MAPKBP1* (c.592C>T (blue) and c.4393C>T (red); **A**) while BN-21 and BN-23 were homozygous for a mutation in *PDE6A* (c.2053G>A; **B**). **C)** Segregation of the *PDE6A* mutation was analyzed by Sanger sequencing. Segregation of *MAPKBP1* mutations is shown in Fig.1.

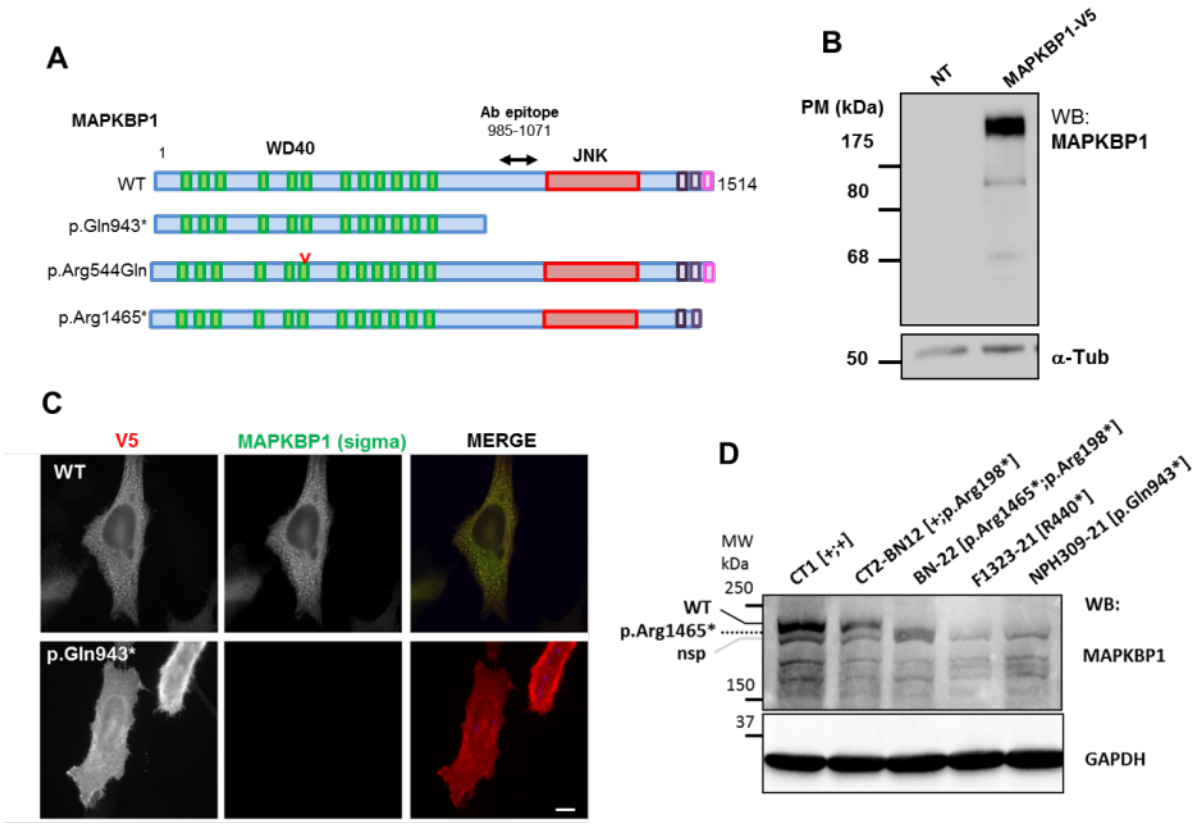

Figure S6: Specificity of the MAPKBP1 antibody.

A) Schema points out the used MAPKBP1 constructs (WT and p.Gln943*) and to the epitope recognized by the Sigma antibody. **B**) Lysates of HEK293 cells transiently transfected or not with the V5-tagged MAPKBP1 encoding plasmid were analyzed by western-blot using a rabbit polyclonal antibody against MAPKBP1 from Sigma (HPA030832; dilution 1/5000) and a mouse monoclonal against alpha-tubulin (clone B-5-1-2, sigma, 1/10.000) as indicated. **C**) HeLa cells transiently transfected with plasmids encoding for V5-tagged WT or p.Gln943* were fixed and stained for V5 (green; mouse monoclonal, clone SV5-Pk1 [AbD Serotec MCA-1360]; dil 1/10.000) and with the MAPKBP1 antibody from Sigma (red). Scale bar: 5 μm. **D**) Lysates of fibroblasts from control (CT1 (healthy unrelated individual), CT2-BN-12) and affected individuals (BN-22, F1323-21, NPH309-21) were analyzed by western-blot using the rabbit polyclonal antibody against MAPKBP1 (HPA030832; dilution 1/1000) and a mouse monoclonal against GAPDH (clone 6C5, Millipore, dil 1/10.000), as indicated. Relative position of full length WT and p.Arg1465* truncated proteins are indicated by black and dotted lanes, respectively. The presence of a nonspecific (nsp) band which migrates just below WT and p.Arg1465* proteins is indicated by a grey lane.

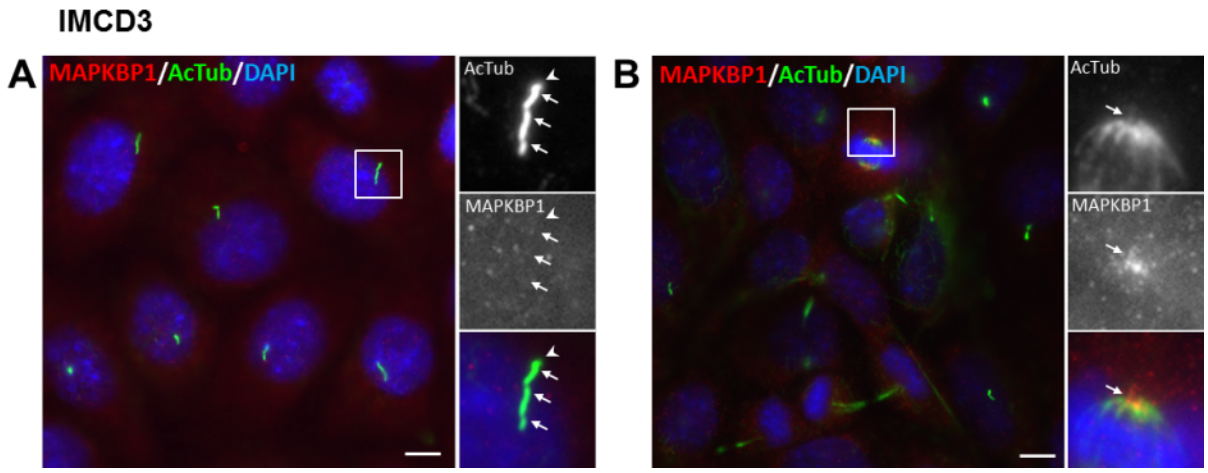

Figure S7: Distribution of MAPKBP1 in ciliated and cycling IMCD3 cells.

Confluent IMCD3 cells were fixed in PFA and stained for acetylated α-tubulin (AcTub, green) and MAPKBP1 (red) similarly as in Figs. 3 and 4. Insets on the right show higher magnifications of representative cilium (**A**) or mitotic spindle pole (**B**) indicated by a white square in the corresponding images. **A**) Arrows indicate cilia, arrowhead cilium base region. **B**) Arrows indicate mitotic spindle pole. Scale bars: 5 μm.

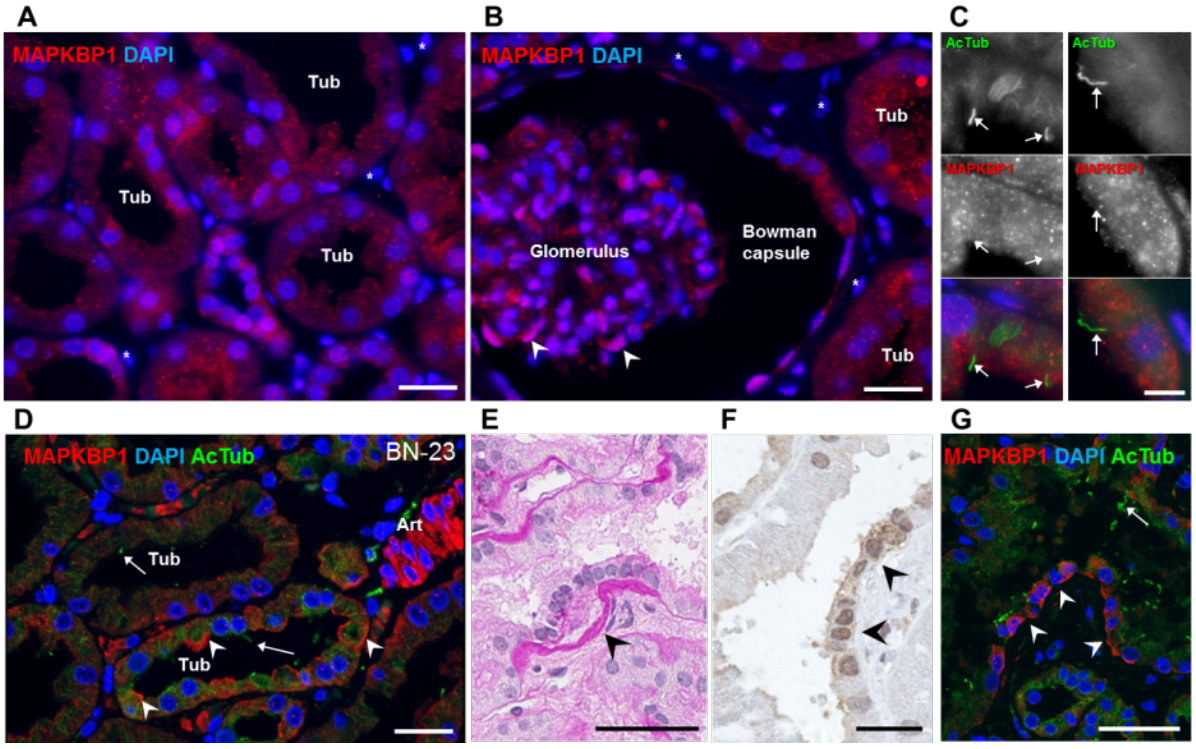

Figure S8: MAPKBP1 shows a diffuse expression pattern in human adult kidney.

A-C) Kidney biopsy from a control individual was stained for MAPKBP1 (red (**A-C**); HPA030832; dil 1/100)) and acetylated tubulin to label cilia (AcTub, green, (**C**); 6–11-B-1, dil 1/500). MAPKBP1 shows a diffuse granular distribution in the cytoplasm of tubular epithelial cells (Tub) as well as in epithelial cells from the Bowman capsule whereas it does not seem to be expressed in interstitial cells (stars). MAPKBP1 is also expressed in cells in glomeruli where it is also found in the nucleus in some cells (arrowheads). MAPKBP1 was not detected in cilia (Arrows). **D)** MAPKBP1 staining (red) in the kidney biopsy of the BN-23 individual. **D** shows tubules (Tub) with focal accentuated staining of tubular epithelial cells and pronounced staining of the smooth musculature of an arteriole (Art). **E-G**) Pictures show a part of proximal tubules with abrupt transition from normal to disorganized basement membrane (**E**, PAS) and to dedifferentiated tubular epithelial cells (arrowheads). This finding is typical but not specific for nephronophthisis. Dedifferentiated tubular epithelial cells express increased positivity for MAPKBP1 (**E**, brown, immunohistochemistry; **G**, red; immunofluorescence). Some cilia are present (**D**, **F**, arrows; AcTub). Scale bars: 20 μm (**A, B, D, F, G**), 50 μm (**E**), 5 μm (**C**).

Figure S9: Injection of *mapkbp1* morpholino does not result in ciliopathy like phenotype.

A-C) Zebrafish embryos were injected with two different *mapkbp1* morpholinos, e2i2 (5'-ATTGAAGTTGAGTTACTCACCCGGC-3') and e4i4 (5'-TTGAGGAATTGAGCACCCACCTCGC-3') targeting exon2:intron2 and exon4:intron4 junctions, respectively. **A)** Efficiency of the used morpholinos on splicing was tested by RT-PCR using primers designed to amplify regions between exon 1 and 3 (e2i2: fw 5'-AGTAAAGCTGGCAACAACAAAGAG-3'/rev 5'-TGCTGTTTGTTCTTCTTAGGGTTC-3') and exons 3 and 5 (e4i4: fw 5'-GAACCCTAAGAAGAACAAACAGCA -3'/rev 5'-CGCCGTATTTATGTTCCTGTAACT-3'). **B)** A representative picture of e2i2 morpholino-injected embryos is shown. **C)** Body axis deformation including curved or deformed) of control and embryos injected with e2i2 or e4i4 morpholinos (1.5mM) was quantified compared to control morpholino-injected embryos (ct). One representative experiment out of two is shown. A morpholino targeting *traf3ip1* (1.5mM) was used in parallel as a positive control and, as expected[4], 85.6% and 83.3% of the injected embryos showed curved body axis and pronephric cysts (not shown), respectively. Experiments on the zebrafish were approved by the "Services Vétérinaires de la Préfecture de Police de Paris" and by the ethical committee of the Paris Descartes University.

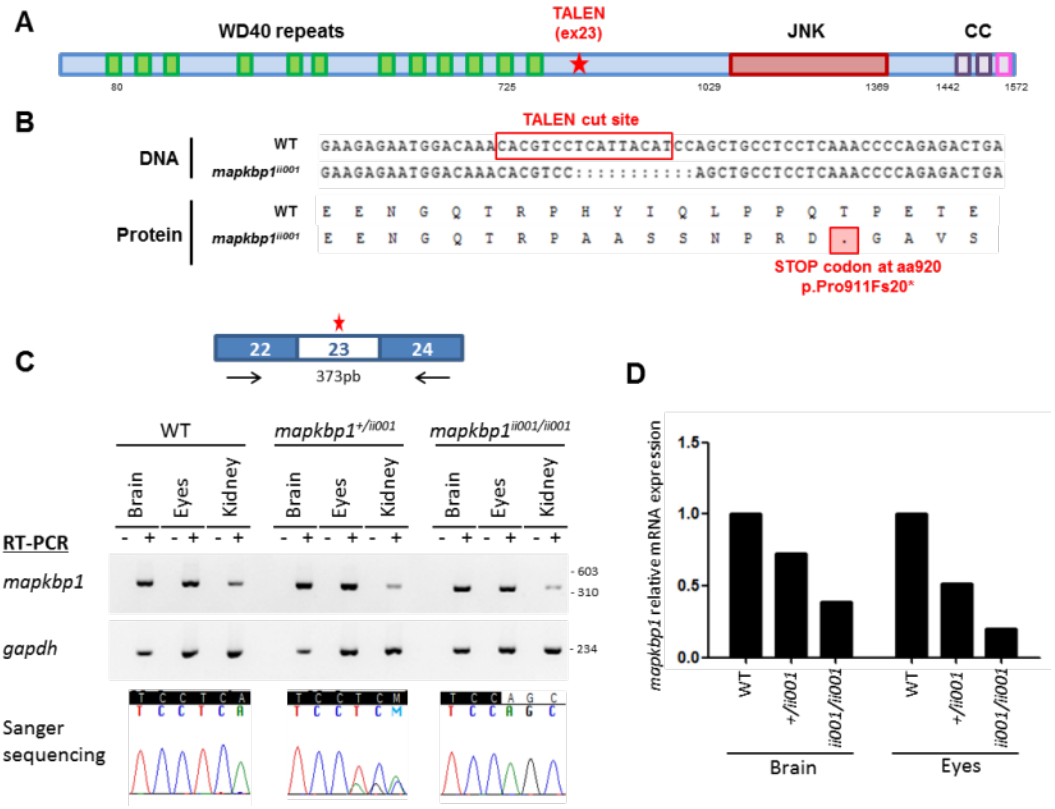

Figure S10: Generation of a *mapkbp1* mutant zebrafish line

A) Schema of Mapkbp1 protein depicting the different functional domains that have been described in the human protein (WD repeats, domain of interaction with JNK, coiled-domain involved in dimerization with WDR62). The TALEN target site in exon 23 is represented in red (star). **B**) DNA and protein sequences of TALEN target site in wild-type and mutated animals. One allele has been identified in F1 generation that deletes 11 base pairs (bp), leading to a frameshift and premature stop codon at amino acid (aa) 920 of zebrafish Mapkbp1 protein. This allele is hereafter referred to as *mapkbp1*^{ii001}. **C**) A 373bp region flanking exon 23 of *mapkbp1* transcript was amplified by RT-PCR from the indicated tissues isolated from WT, heterozygous and homozygous mutant adult (7-month old) fish using primers in exons 22 and 24 (mapkbp1-RTex22_F 5'-TCCATGTTGGACCTGAGACA-3'; mapkbp1-RTex24_R 5'-ACAGGCGACTGCTGGAATAC-3'). *gapdh* was amplified as a positive control (gapdh_F 5'-GTTGGTATTAACGGATTCGGTC-3'; gapdh_R 5'-CACTTAATGTTGGCTGGGTC-3'). Chromatograms from Sanger sequencing of of the TALEN cut site (black) of RT-PCR products from WT, heterozygous and homozygous mutant fishes are shown at the bottom. These data indicate that there is no exon skipping of exon 23 and that the mutation is expressed. **D)** qRT-PCR (SybR Green PCR Master mix, Applied Biosystems) analysis of *mapkbp1* relative expression in WT, heterozygous and homozygous mutant fish show a 80 % (Eyes) and 60% (Brain) decrease compare to WT tissues, indicating RNA decay. *mapkbp1* expression was normalized to *ef1α* expression (mapkbp1-qPCR_F 5'- GGGCTGCTCTGTGAGTTCAA-3'; mapkbp1-qPCR_R 5'- GTGGCCATACTGGTTGCGA-3'; ef1α-qPCR_F 5'- CTGGAGGCCAGCTCAAACAT-3'; ef1α-qPCR_R 5'- ATCAAGAAGAGTAGTACCGCTAGCAT-3'). Of note, expression of *mapkbp1* in kidney tissues was not detectable by qPCR.

Figure S7

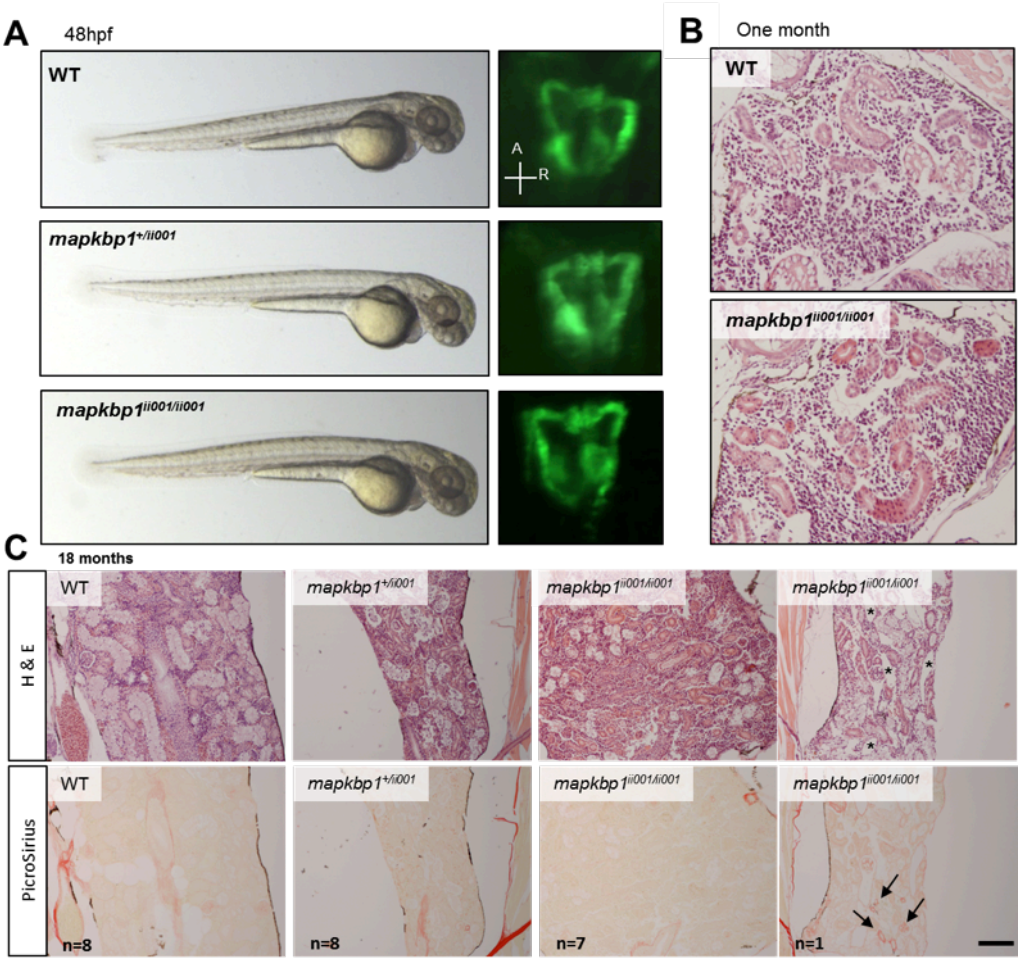

Figure S11: *mapkbp1*$^{ii001/ii001}$ mutant zebrafish embryos do not present ciliopathy-related phenotype

A) *mapkbp1*$^{ii001/ii001}$ mutant animals do not show any obvious phenotype at embryonic (here shown at 48hpf) and larval stages. *Tg(wt1b:GFP)* transgenic embryos allow the visualization of proximal pronephros, that look normal in mutant embryos (dorsal views, anterior (A) to the top). Mutant animals survive till adulthood and are fertile. Maternal-zygotic mutant embryos do not have obvious phenotype either. **B-C**) Histological analysis (H&E) of one-month (B) and 18-month (C) old WT, heterozygous and *mapkbp1*$^{ii001/ii001}$ kidneys revealed no noticeable abnormalities, except in one of the eight aged mutant animals which exhibited tubular dilations (*) associated with slight fibrosis as shown by PicroSirius staining (**C**, right panel; arrows). Scale bar, 200µm.

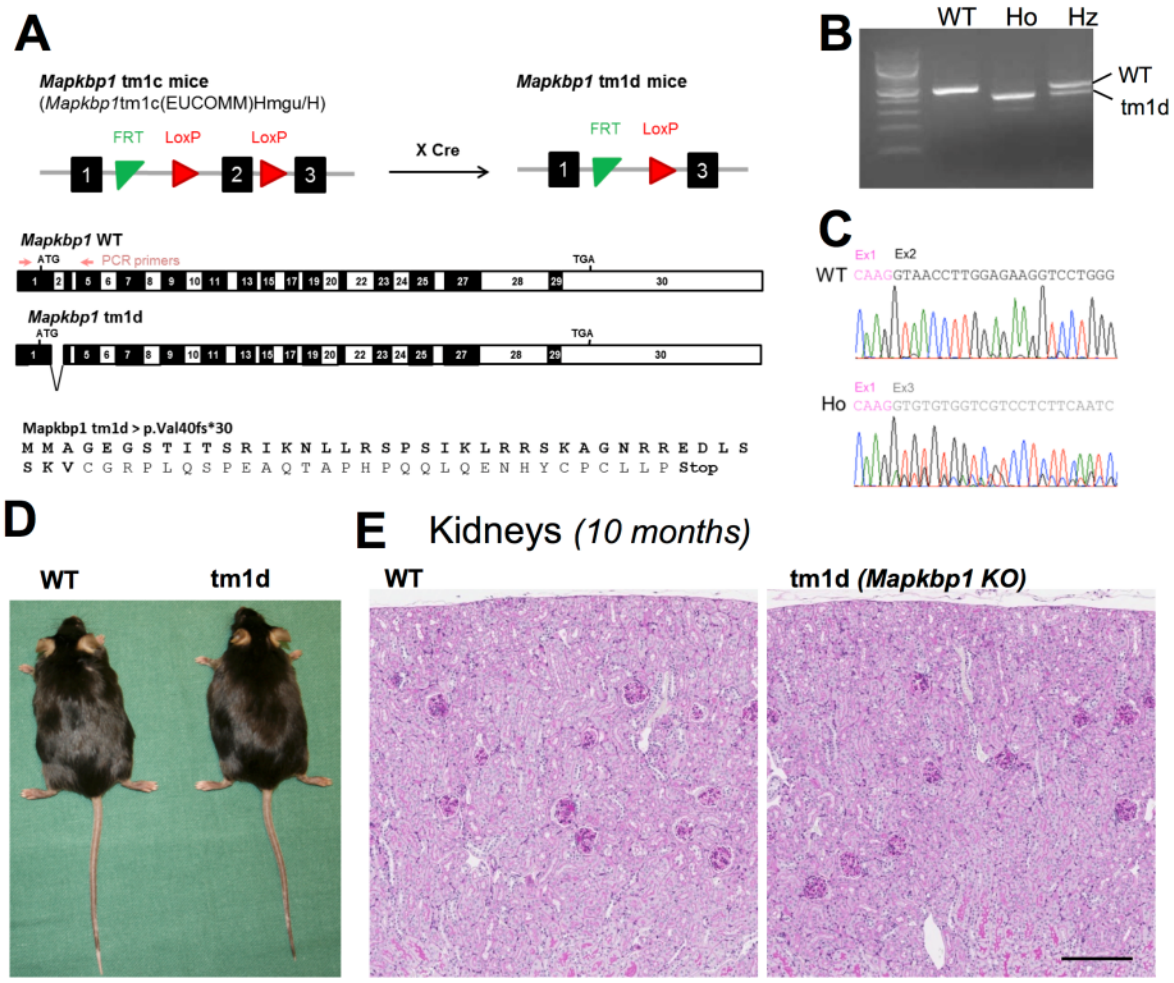

Figure S12: mRNA expression and morphology of kidneys from *tm1d Mapkbp1* mice.

A) *Mapkbp1* tm1c mice (*Mapkbp1*tm1c(EUCOMM)Hmgu/H) and Cre-expressing mice (C57BL/6NTac-Tg(ACTB-cre)3Mrt/H) were obtained from MRC-Harwell (UK) and bred to generate *Mapkbp1* tm1d mice. In the tm1c mice, exon 2 of *Mapkbp1* is flanked by two LoxP sites (http://www.mousephenotype.org/data/alleles/MGI:1347004/tm1c(EUCOMM)Hmgu/) which was then exised by the Cre recombinase. Exon2 is 92 nucleotides long, it is not in frame and its deletion is predicted to lead to frame shift with introduction of a stop codon 30 aminoacids after p.Val40. **B**) RT-PCR analysis of *Mapkbp1* expression. RNA was extracted from kidneys of wild-type (WT), heterozygous (Hz) or homozygous (Ho) mice and the exon1-exon5 region was amplified by RT-PCR (MAPKBP1-mus-cds-1-1F 5'-catatccgaaggctgtgttg-3', MAPKBP1-mus-cds-1-1R 5'-tagctctgccacctggctac-3'). The cDNA from the mouse homozygous for the *Mapkbp1* tm1d allele has a shorter transcript compared to WT corresponding to the lack of exon 2. **C**) Chromatograms from Sanger sequencing of PCR products from homozygous and WT mice obtained as in **B**. Sequences corresponding to exon 1 are indicated in pink whereas exon 2 and exon 3 are indicated in black and grey respectively. **D**) Pictures of representative WT and tm1d Mapkbp1 KO mice. **E**) Histologic examination (PAS staining) of kidneys of wild-type (WT) and homozygous (*Mapkbp1* KO) 10 months of age mice shows no pathology. Scale bar: 200 μm. Works on mice were approved by the Norwegian Food Safety Authority (FOTS 8367).

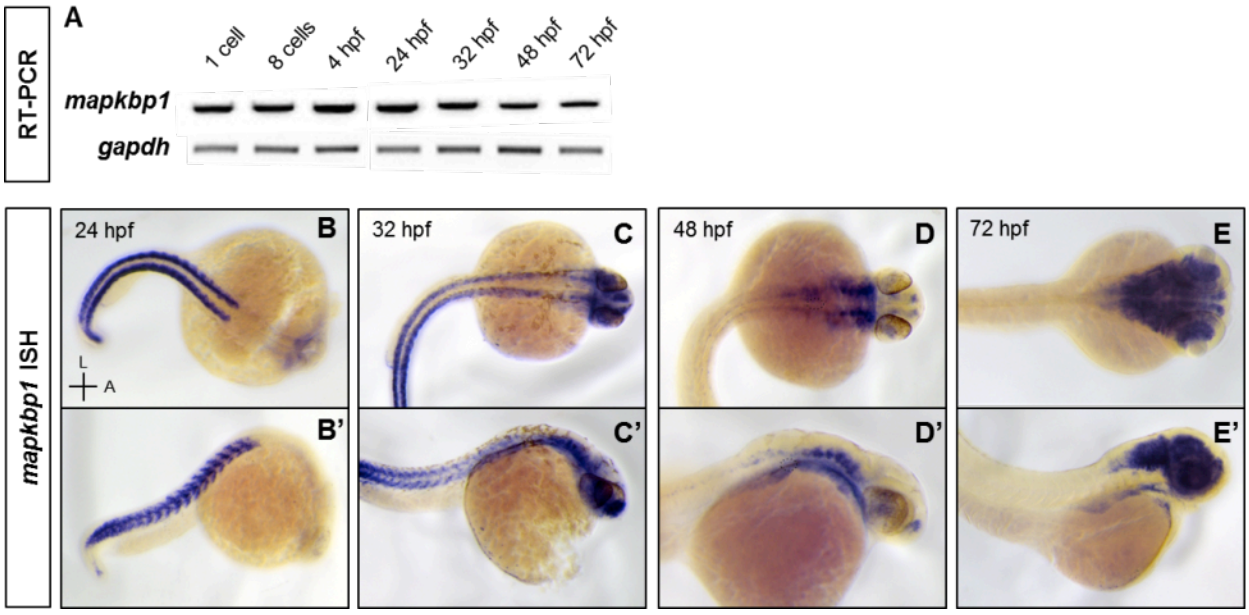

Figure S13: Expression pattern of *mapkbp1* during zebrafish early development

A) RT-PCR analysis of *mapkbp1* expression performed on WT zebrafish embryos. Expression at 1-cell and 8-cell stages indicate a maternal contribution of *mapkbp1* transcripts. **B-E**) Whole mount *in situ* hybridization of *mapkbp1* at 24, 32, 48 and 72 hours post fertilization (hpf). At 24 hpf, a strong expression is observed in the somites and then in the head at 32 hpf. From 48 hpf, *mapkbp1* expression starts to be restricted to the brain. Noteworthy, no expression is detected in the pronephros during embryonic developmental stages. Dorsal (top, **B-E**) and lateral (bottom, **B'-E'**) views, anterior to the right.

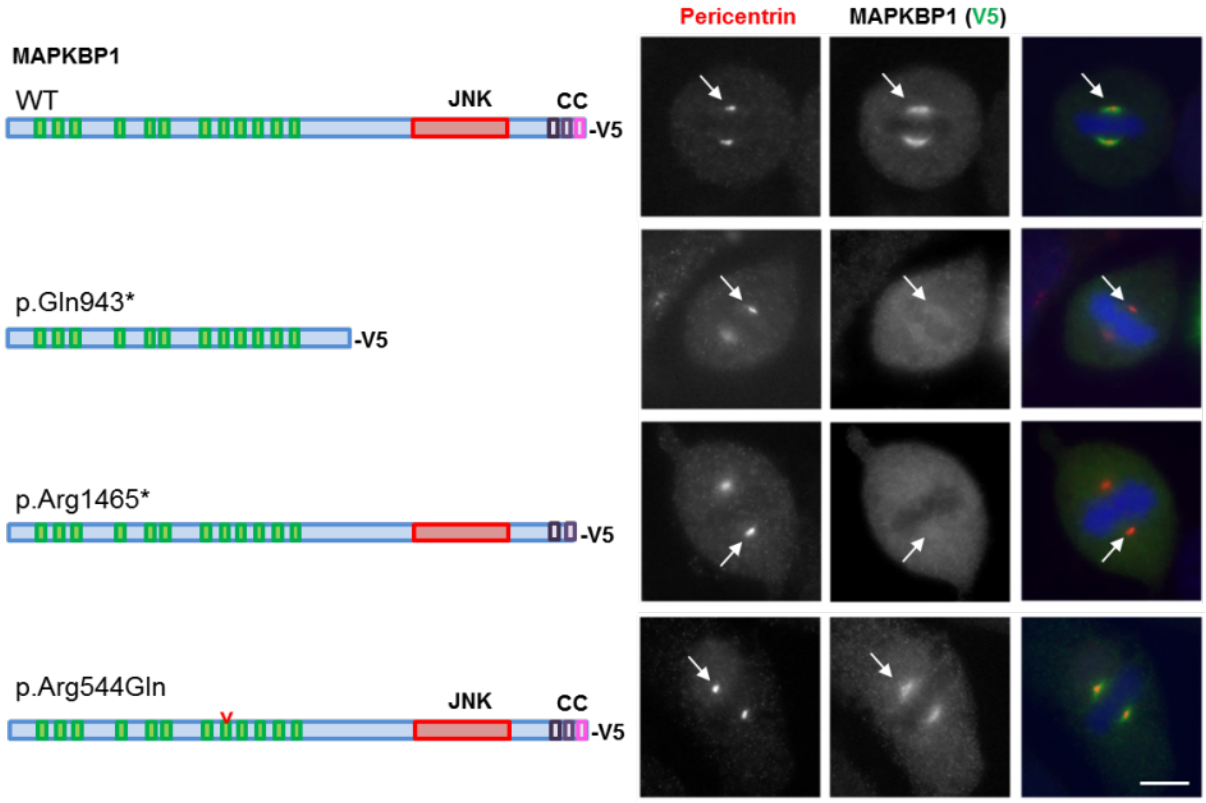

Figure S14: Impact of mutations on the targeting of MAPKBP1 to mitotic spindle poles.
HeLa cells transiently transfected with indicated MAPKBP1 WT and mutant V5-tagged constructs were fixed in PFA (4%) and stained for pericentrin (red; rabbit polyclonal, Abcam ab4448, dil 1/3.000) and V5 epitope (MAPKBP1, green; mouse monoclonal, clone SV5-Pk1, AbD Serotec MCA-1360, dil 1/10.000).

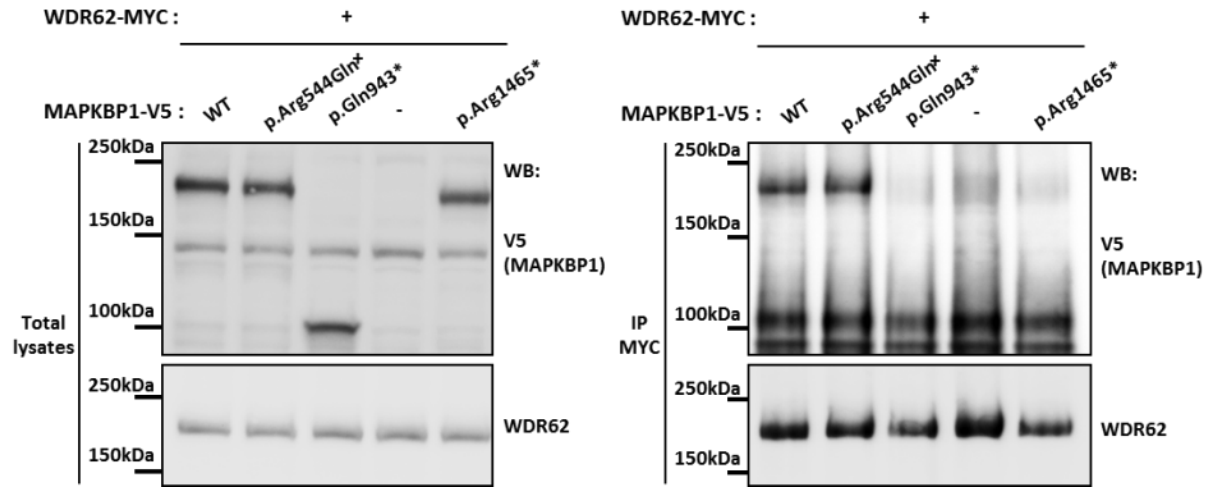

Fig.S15: Impact of *MAPKBP1* mutations on the interaction with WDR62.

HEK293 cells were transiently transfected (lipofectamine [ThermoFischer]) with plasmids encoding V5-tagged WT and mutant forms of MAPKBP1 and Myc-tagged WDR62, as indicated. Cells were lyzed and immunoprecipitated with the anti-myc antibody (MYC: mouse monoclonal, Ab-2 clone 9E10.3 [Fisher Scientific MS-139-P1]). Lysates and immunoprecipitates (IP) were analyzed by western-blot as indicated (WB; V5: Mouse monoclonal clone SV5-Pk1 [AbD Serotec MCA-1360], dil 1/5000; WDR62: rabbit polyclonal [NB100-77302, NOVUS], dil 1/5000).

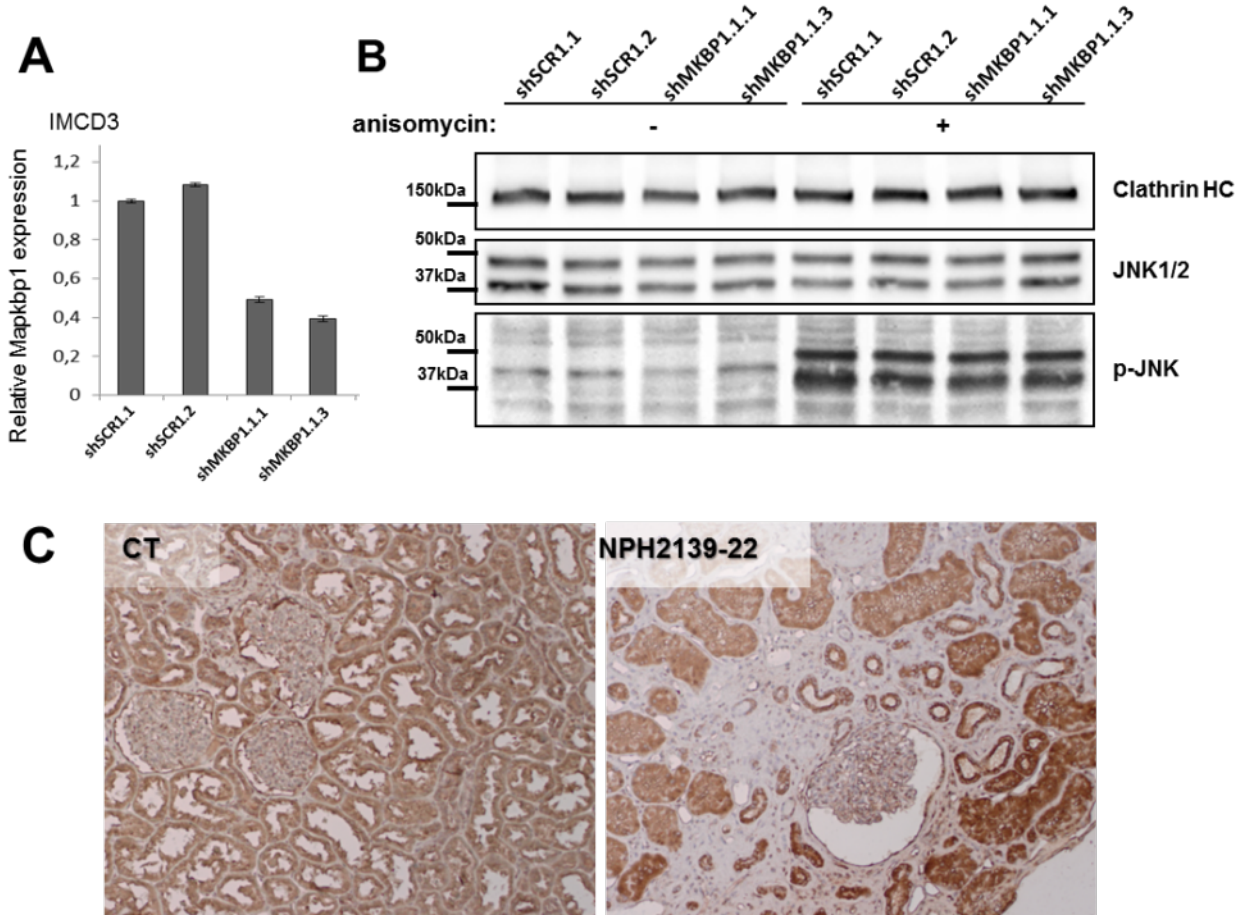

Figure S16: JNK signaling is not altered in *MAPKBP1* mutant conditions.

A) IMCD3 cells were stably transduced by a lentiviral vector (pLKO.1-TRC vector; https://www.addgene.org/8453/) expressing either scrambled or *Mapkbp1* (Sh#5: 5'-CCAGTCAACAACCTTCTCCAA–3') targeting shRNA. Expression of *Mapkbp1* (mMKBP1-qPCR-20F: 5'CCAGCTCTGCCCATCCTT-3'; mMKBP1-qPCR-22R: 5'-TCCAGGTACTCCATGGTCTCTTG-3') measured by quantitative RT-PCR was normalized to *Hprt* (mHPRT-qPCR-F: 5'-AGGGCATATCCAACAACAACCTT-3'; mHPRT-qPCR-R: 5'-GTTAAGCAGTACAGCCCCAAA-3') expression in both control (shSCR1.1, shSCR1.2) and *Mapkbp1* (shMKBP1.1.1; shMKBP1.1.3) IMCD3 clones. **B**) IMCD3 cell lines expressing scrambled or Mapkbp1 targeting shRNA were treated or not with anisomycin (1,25ng/µl) for 1h, then lyzed and analyzed by western-blot using antibodies against clathrin heavy chain (HC, loading control; rabbit polyclonal, Abcam ab21679, dil 1/5000), JNK1/2 (clone 252323, R&D system, 1/5000) or phosphorylated JNK (p-JNK; AF1205, R&D system , 1/5000). **C**) Kidneys from control and from NPH2139-22 individuals with an antibody against phosphorylated Jun (p-c-Jun; 9261S, cell signaling, 1/50).

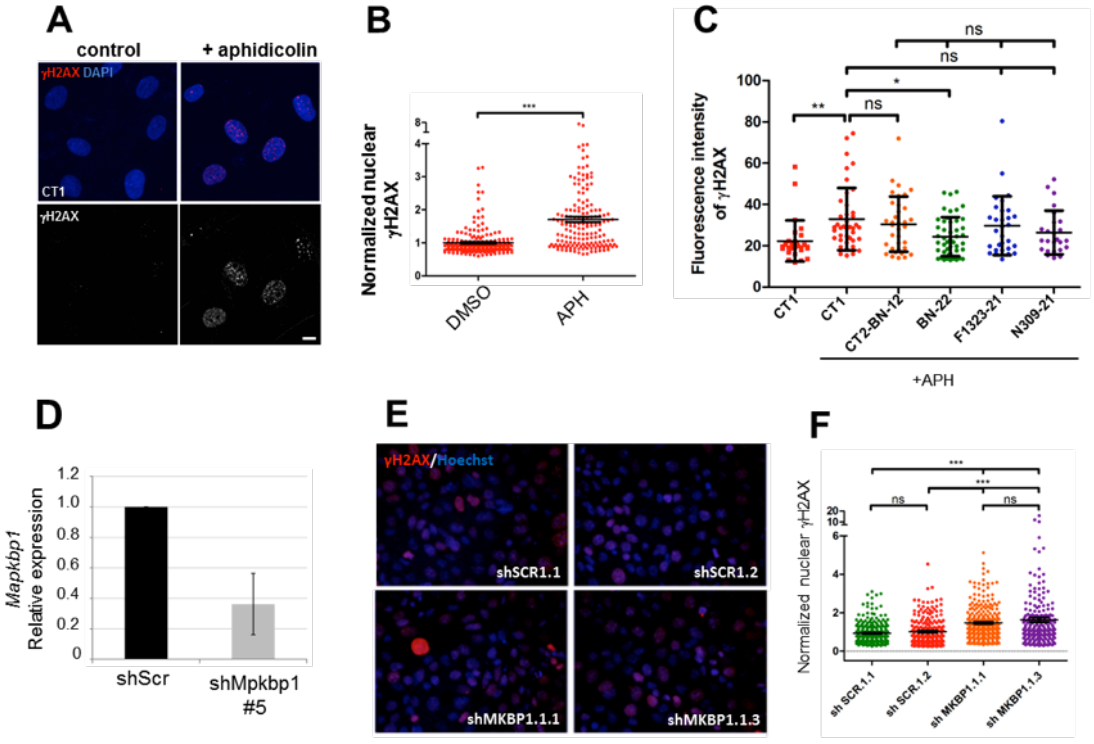

Figure S17: Effect of MAPKBP1 mutations or knockdown on DDR signaling.

(A) Fibroblasts from control individual (CT1) were treated or not with aphidicolin (APH; 400 nM, 24hrs) fixed (PFA) and stained for phosphorylated γH2AX (red; mouse monoclonal, clone JBW301 [MILLIPORE 05-636], 1/200) together with DAPI (blue). **(A)** Intensity of nuclear γH2AX staining was quantified from three independent experiments using imageJ (n: DMSO=233, APH=167). ns and ***p < 0.0001 were calculated via Dunn's Multiple Comparison Test after the analysis of variance ANOVA test. Scale bar, 5μm. (**C**) Fibroblasts from controls and affected individuals were treated with APH fixed and stained for phosphorylated γH2AX and intensity of nuclear γH2AX staining was quantified as in (**A**). One representative experiment out of two is shown (n>25). Ns, *p < 0.01 and **p < 0.001 were calculated via Dunn's Multiple Comparison Test after the analysis of variance ANOVA test. (**D**) Expression of *Mapkbp1* was measured in NIH 3T3 cells clones expressing scrambled (shSCR) or Mapkbp1 (shMapkbp1#5) targeting shRNA (**Figure S16**) by quantitative RT-PCR and normalized to *Gapdh* expression. Error bars indicate s.d., derived from four independent experiments. (**E, F**) IMCD3 cells clones expressing scrambled (shSCR) or Mapkbp1 (shMKBP1) targeting shRNA (**Figure S16**) were analyzed similarly as in **Figure 7**. IMCD3 cells were fixed and stained for γH2AX (red) together with DAPI (blue). The intensity of nuclear γH2AX staining was quantified from three independent experiments (n>220). ns and ***p < 0.0001 were calculated via Dunn's Multiple Comparison Test after the analysis of variance ANOVA test.

Supplementary tables

	F1323-21	A3977-22	BN-22/23	NPH309-21	NPH2139-21
Next generation sequencing	Whole exome				Ciliome
Total variants called	451,846	340,459	18,315	54,781	5,983
Coding and splice site variants excluding synonomous variants	/	/	8,686	14,344	885
rare variants (not in in-house databases or dbSNP132 and 1KG, MAF<0.5%)	1,680	2,275	232	188	32
Linkage analysis (Figure S1)	170	142	/	6	/
Quality filtering ; Compound heterozygote or homozygote variants (recessive disease model)	/	/	10	1	3
Surviving variants to evaluation	24	15	10	1	1

Table S1: Candidate gene selection from whole exome or ciliome resequencing in affected individuals. The number of variants that remained after filtering strategy (see below for each family), are shown for each individual. A quality filter was applied for all variants: all calls with a read coverage ≤ 2 and a Phred-scaled SNP quality of ≤ 20 were filtered out.

For F1323-21 and A3977-21 individuals, WES and variant burden analysis was performed as previously described[5] using Agilent SureSelect human exome capture arrays (Life Technologies) with next generation sequencing (NGS) on an Illumina HiSeq sequencing platform. Sequence reads were mapped against the human reference genome (NCBI build 37/hg19) using CLC Genomics Workbench (version 6.5.1) software (CLC bio). The average coverage was 62 X with 96% of target bases covered at least 10 X. Variants with minor count <2 and with minor allele frequencies <1% in the dbSNP (Version 137) database were selected and annotated for impact on the encoded protein and for conservation of the reference base and amino acid among orthologs across phylogeny. Mutation calling was performed by geneticists/cell biologists, who had knowledge of the clinical phenotypes and pedigree structure, as well as experience with homozygosity mapping and exome evaluation.

For family BN (BN22-BN23), WES was performed at HudsonAlpha Institute for Biotechnology (Huntsville,AL) using Roche-NimbleGen Sequence Capture EZ Exome v2 kit and paired-end 100nt sequencing on the Illumina HiSeq, analyzed with Casava v1.8 (Illumina Inc) and aligned to the hg19 reference genome using Burrows-Wheeler Aligner (BWA) to a total of 74 X median coverage of the target capture regions with more than 93% of target bases covered at least 20 X. Variant calling (coding and putative splice sites) was performed as described elsewhere[6]. Coding variants and variants in putative splice sites were further filtered against variants identified in 300 Norwegian exome-resequencing samples and variants present at >0.5 % allele frequency in the 1000 Genomes database.

For the NPH309-21 affected individual, WES and variant burden analysis was performed as described previously[7]. The raw data FASTQ files were first mapped to NCBI build 37/hg19 reference genome using 'BWA'. Duplicated reads were removed using 'Samtools'. BAM files were processed by Genome Analysis Toolkit (GATK) to make local realignment and base score recalibration. GATK's UnifiedGenotyper module was used to call variants. Run GATK to generate VQSLOD score for each variant. Run VEP to annotate the effect of the variants. The average coverage is 86X. Nearly 6M variants were generated by GATK. ~97.5% of target exome regions have coverage > 10x.

Ciliary exome targeted sequencing and bioinformatics filtering conducted in NPH2139-21 individual was performed using a custom SureSelect capture kits (Agilent Technologies) targeting 4.5 Mb of 20,168 exons (1 221 ciliary candidate genes), including MAPKBP1[4]. Briefly, Agilent SureSelect librairies were prepared from 3 µg of 300 genomic DNA samples sheared with a Covaris S2 Ultrasonicator according to manufacturer's instructions. The Ovation Ultralow System (NuGEN Technologies) was used to prepare HiSeq2500 pre-capture barecoded libraries. The ciliome capture by hybridization was performed on a pool of 10 to 16 barecoded precapture libraries. Sequencing performed on HiSeq2500 (Illumina) was done on pools of barcoded ciliome librairies (16 ciliome libraries per lane of HiSeq FlowCell). Paired-end reads were generated (100+100) and mapped on human genome reference (NCBI build37/hg19 version) using BWA. Downstream processing was carried out with the GATK, SAMtools, and Picard Tools, following documented best practices (http://www.broadinstitute.org/gatk/guide/topic?name=best-practices). All variants were annotated using a software system developed by the Paris Descartes University Bioinformatics platform. The mean depth of coverage obtained was 112x, and more than 91% of the exome was covered at least 30x. A quality filter was applied for all variants: all calls with a read coverage ≤ 2 and a Phred-scaled SNP quality of ≤ 20 were filtered out. Different filters were applied to exclude all variants located in non-exonic regions, pseudogenes, UTRs or known polymorphic variants with a frequency above 1%, i.e. present in databases such as dbSNP, 1000 genome projects and all variants identified by in-house exome sequencing (8445 exomes and 1289 ciliomes).

The functional consequences of missense variants was predicted using SIFT (http://sift.jcvi.org/www/SIFT_enst_submit.html), PolyPhen2 (http://genetics.bwh.harvard.edu/pph2/) and mutation taster (http://www.mutationtaster.org/) softwares.

Table S2 : Overview of bi-allelic variants identified from exome or ciliome data in affected individuals.

Genes written in bold letters indicate likely disease-causative variants. Segregation analysis revealed that *MAPKBP1* variants segregate with disease in these families (shown in the pedigree in Fig.1). Columns from left to right: position of the variant in hg19 (genomic position), chromosome (chr), name of the gene in which the variant is detected (Gene), RefSeq accession, nucleotide (Nt) and amino acid (AA) change, Polyphen 2 (PP2) and SIFT Score (red : predict disease causing, yellow: intermediate, green: predict benign), homozygotes (hom) or heterozygotes (het) variants, number of reads whereby position is covered for reference allele (Ref) and variant allele (var), genes and variants reported in Biobase/HGMD and associated disease, allelic frequency in Exome Aggregation Consortium (ExAC), validation by Sanger sequencing (Sanger), variant segregate with disease (Segregation). [a]Variant does not occur homozygously in ExAC. [b]IDH3B was previously reported to cause Retinitis pigmentosa when defective. However, this association is only based on a single publication with 2 affected families[8].

References:

1. Schuetz, A., Allali-Hassani, A., Martín, F., Loppnau, P., Vedadi, M., Bochkarev, A., Plotnikov, A.N., Arrowsmith, C.H., and Min, J. (2006). Structural basis for molecular recognition and presentation of histone H3 by WDR5. EMBO J. *25*, 4245–4252.

2. Ruthenburg, A.J., Wang, W., Graybosch, D.M., Li, H., Allis, C.D., Patel, D.J., and Verdine, G.L. (2006). Histone H3 recognition and presentation by the WDR5 module of the MLL1 complex. Nat. Struct. Mol. Biol. *13*, 704–712.

3. Cartegni, L., Wang, J., Zhu, Z., Zhang, M.Q., and Krainer, A.R. (2003). ESEfinder: A web resource to identify exonic splicing enhancers. Nucleic Acids Res. *31*, 3568–3571.

4. Bizet, A.A., Becker-Heck, A., Ryan, R., Weber, K., Filhol, E., Krug, P., Halbritter, J., Delous, M., Lasbennes, M.-C., Linghu, B., et al. (2015). Mutations in TRAF3IP1/IFT54 reveal a new role for IFT proteins in microtubule stabilization. Nat. Commun. *6*, 8666.

5. Boyden, L.M., Choi, M., Choate, K.A., Nelson-Williams, C.J., Farhi, A., Toka, H.R., Tikhonova, I.R., Bjornson, R., Mane, S.M., Colussi, G., et al. (2012). Mutations in kelch-like 3 and cullin 3 cause hypertension and electrolyte abnormalities. Nature *482*, 98–102.

6. Haugarvoll, K., Johansson, S., Tzoulis, C., Haukanes, B.I., Bredrup, C., Neckelmann, G., Boman, H., Knappskog, P.M., and Bindoff, L.A. (2013). MRI characterisation of adult onset alpha-methylacyl-coA racemase deficiency diagnosed by exome sequencing. Orphanet J. Rare Dis. *8*, 1.

7. Boyer, O., Woerner, S., Yang, F., Oakeley, E.J., Linghu, B., Gribouval, O., Tête, M.-J., Duca, J.S., Klickstein, L., Damask, A.J., et al. (2013). LMX1B mutations cause hereditary FSGS without extrarenal involvement. J. Am. Soc. Nephrol. JASN *24*, 1216–1222.

8. Hartong, D.T., Dange, M., McGee, T.L., Berson, E.L., Dryja, T.P., and Colman, R.F. (2008). Insights from retinitis pigmentosa into the roles of isocitrate dehydrogenases in the Krebs cycle. Nat. Genet. *40*, 1230–1234.